Simple Book Example

TeXstudio Team

January 2013

thesis

Contents

List of Figures

Chapter 1

Simulations of a plenoptic 1.0 system

In this chapter we present some results obtained simulating raw data images using the simulation platform described in chapter **??**. We also describe how we used the digitally generated light fields data to design, develop and test the data processing algorithms, such as the rendering, the synthetic refocus and the depth estimation algorithms. Light fields are generated from the raw images obtained propagating light in the system using the methods described in chapter **??**. All the light field processing algorithms use the third parametrization of the light field, described in **??**, that is the four dimensional array of the intensity recorded on the sensor whose indexes are the position x and y, and the the direction θ_x and θ_y.

1.1 Description of the system

The plenoptic 1.0 camera described in section **??** has been modelled with a simple 2f system composed by a main lens, a micro lens array and a sensor as shown in figure 1.1. The micro lens array is placed at a distance $z = 2f$

form the main lens, where f is the focal length of the main lens, and the sensor is placed at a distance f_μ from the micro array plane that is also the focal length of the lens lets. In this configuration the lens let array plane is conjugated with the object plane, while the sensor plane is conjugated with the main lens plane. In order to satisfy the f-number matching condition described in section **??** once fixed the propagation distances, the micro lens array parameters, the resolution N of the input field and the wavelength of the light used and the micro array parameters, the software automatically sets the aperture of the main lens.

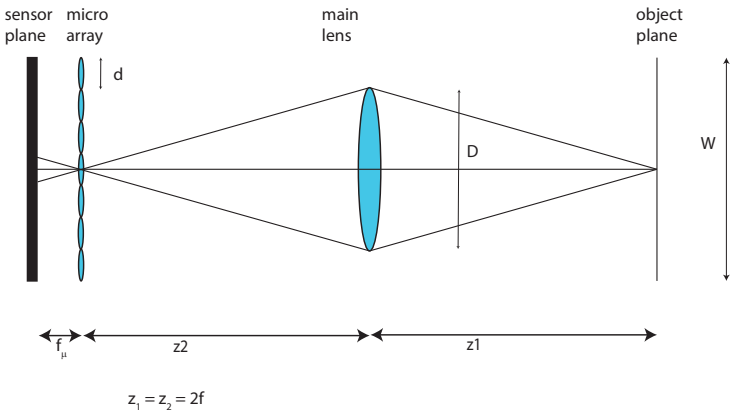

Figure 1.1: The parameters that characterize the micro lens array are: the pitch p, defined as the distance between the centres of two neighbours lens lets, the diameter d, the number of lens lets per raw N and the size of the micro array W.

The micro array parameters are illustrated in figure 1.2. Those are the pitch between two close lens lets, the diameter of the single lens let, the number of lens let in a row and the size of the array. In all our simulations the pitch of the lens lets is taken equal to the size of its diameter and the lens lets are arranged in a square matrix.

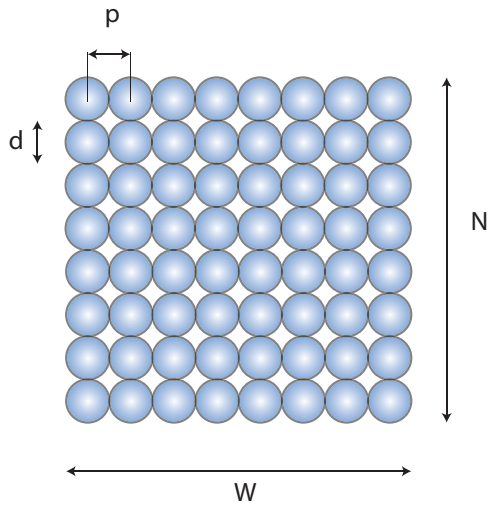

Figure 1.2: The parameters that characterize the micro lens array are: the pitch p, defined as the distance between the centres of two neighbours lens lets, the diameter$d$, the number of lens lets per raw N and the size of the micro array W.

1.1.1 Diffraction effects on the System

Diffraction form the lens let circular aperture generates cross talk between neighbours sub images since the light form a single lens let falls in the sub image of the neighbour lens let. Because of this, blur is present in the rendered image with a consequent loss of spatial resolution. To avoid this loss of resolution the diameter of each lens let should be larger enough so that the size of the Airy disk diffraction pattern is totally included into a single sub image. As seen in equation **??** for a lens with a circular aperture, the diameter of the Airy disk at it's focal plane is

$$d_{Airy} = 1.22\lambda z/D \tag{1.1}$$

We assume that in order to avoid diffraction induced cross talk the lens let diameter should be at least twice the Airy disk diameter so that the

diffraction pattern is included in the sub image until its second zero. We have:

$$D > 2.44\frac{\lambda z}{D} \tag{1.2}$$

Therefore the condition of D is:

$$D > \sqrt{2.44\lambda f_{\mu}} \tag{1.3}$$

Therefore when choosing a or designing a lens let array for plenoptic imaging, the lens let diameter and the focal length should satisfy equation 1.3. The acceptable values belongs to the area above the blue line in the diagram shown in figure 1.3.

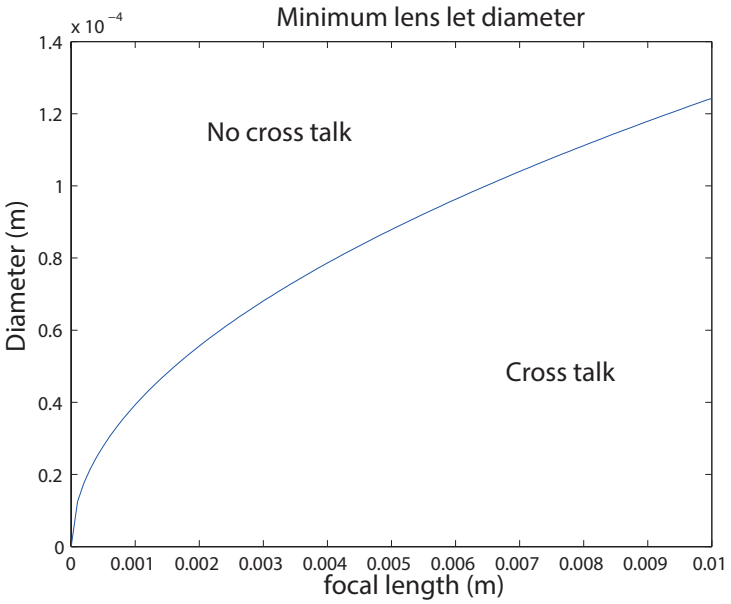

Figure 1.3: Values of acceptable lens let diameter to avoid diffraction induced cross talk.

The effect of cross talk between lens lets on the raw image is shown in figure 1.4.

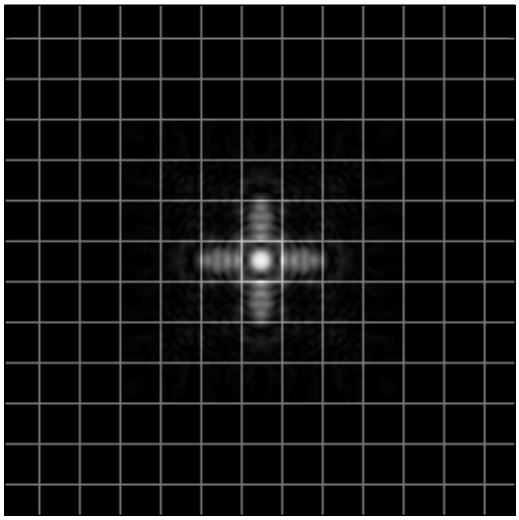

Figure 1.4: Raw image of a point source.The grid represents the edges of the sub images. If the point source is in focus, it should be represented by only one lens let. Because of diffraction some light goes also on the neighbours sub images.

Figure 1.5 shows what happen in the phase space of point source in presence of cross talk and without cross talk. In the first case there is no blur since all the light coming from a point source in focus is recorded by a single lens let, while in the second case the spreading of the light due to diffraction causes a blur that is proportional to the number of sub images involved.

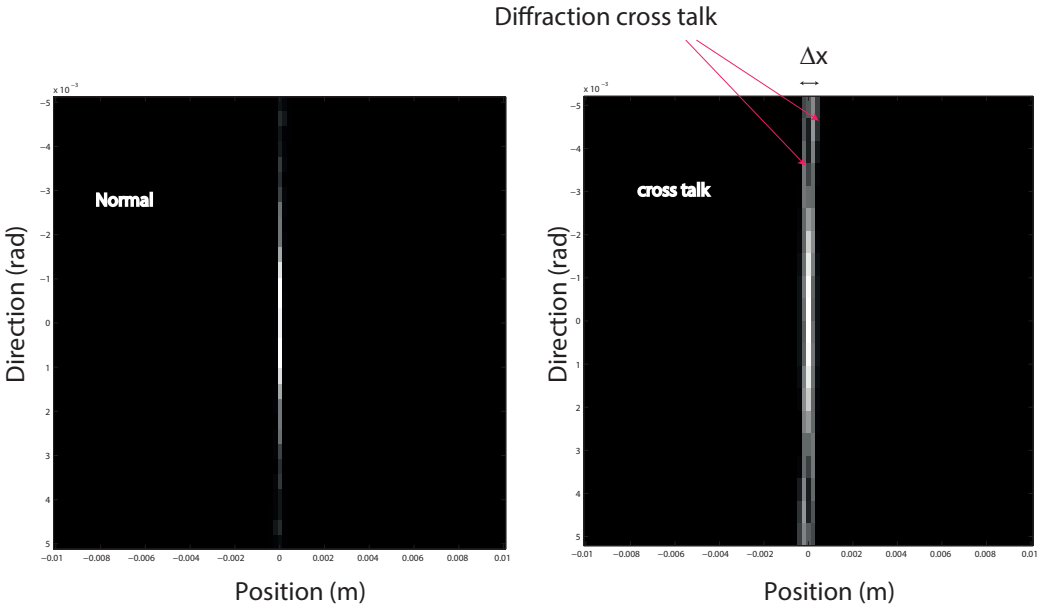

Figure 1.5: Phase space of a single point light field: on the left when the condition 1.3 is respected; on the right when diffraction induces cross talk arise between neighbours lens lets. cross talk introduces a blur in the rendered image whose width is Δx.

Uncdrtinty of one lenslet is too much due to low resolution of plenoptic 1.0, because we are exploring plenoptic in microscopy so spatial resolution is important as well. explore plenoptic at diffraction level. Algorithms are defined by geometrical optics so they dont work anymore if diffraction is too strong

1.2 Advanced Rendering Techniques

As described in chapter **??**, one pixel in the rendered image is obtained as a mean of all the pixels of a the sub image that corresponds to the position of the pixel in the final image. This methods generates an image that is equivalent to the image obtained with a conventional camera without any additional information. In addition to that since the final resolution depends on the number of lens lets in the micro array, it will be smaller than the resolution that can be obtained by a conventional camera which instead uses

the full sensor resolution [3]. To use the full variety of features enabled by light field imaging, more advanced porst processing techniques of the raw data should be used. The first two post processing features we present are the change of aperture and of point of view. These effects are achieved integrating the each sub image along a sub set of directional coordinates, hence on a smaller number of pixels.

1.2.1 Changing Aperture

The quality of the image captured by a conventional camera depends, with a lot of simplifications, by the combination of shutter speed and aperture chosen in order to get the optimum total exposure [23]. The possibility to change the aperture of the main lens in post processing is a vary useful and interesting feature since allows to change the depth of field of the final image. In our simulations the shutter speed is not an issue since all the objects imaged where static with constant and uniform illumination. Therefore what determine the exposure is the aperture of the main lens or the f-number. The f-number is proportional to the depth of field of the imaging system that can be defined as the range of depths that appears sharp in the resulting photograph [2]. If the f-number increases and the aperture gets smaller, the depth of field increases. Therefore a plenoptic camera can control the depth of field in post processing. If we look at the raw plenoptic image, each sub image is formed by a number of samples of the directions of the rays. If in equation **??** we reduce the range of integration along the directional coordinates, this is equivalent in reducing the aperture of the main lens, because if the aperture is smaller rays propagating with an high angle respect the optical axis will

not reach the sensor. Therefore they will be not considered to form the intensity of each pixel. The result is a rendered image that looks like it has been captured with a narrower aperture. From a computational point if we want to reduce the aperture of a k pixels we have:

$$I(x,y) = \frac{1}{N'^2} \sum_{i=k/2}^{N-\frac{k}{2}} \sum_{j=k/2}^{N-\frac{k}{2}} L(x,y,i,j) \tag{1.4}$$

where $N' = N - k$. This operation in the phase space is shown in figure:

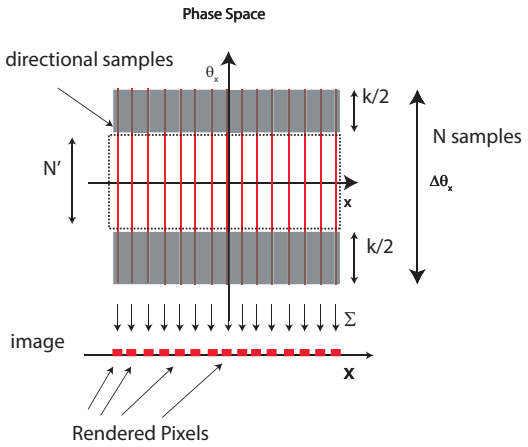

Figure 1.6: Rendering seen from the (x, θ_x) slice of the phase space. In grey are shown the directional pixels not considered for the integration.

An example of implementation of the change of the aperture can be seen in figure 1.7. The two images has been rendered from the raw data described in section **??**.

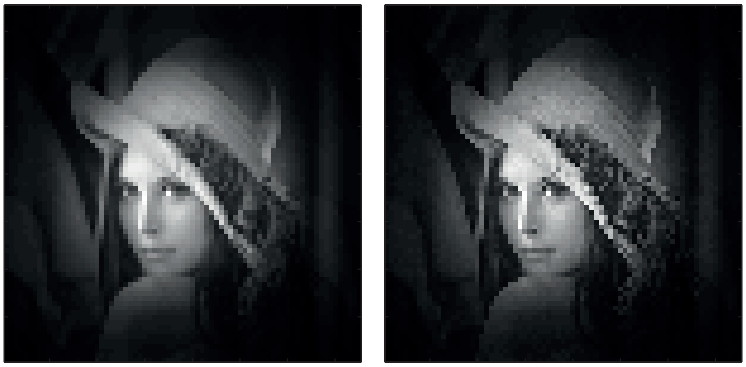

Figure 1.7: The two images are rendered from the same raw data. The image on the left has been rendered integrating along all the sub image, while the image on the right has been rendered taking only the central pixel form each sub image. Since the object is a 2 dimensional image, the effect on the depth of field is not present.

The object, as explained in section **??**, is a two dimensional picture, the extended depth of filed is not noticeable. What can be quantified is the amount of light present in the two images. With full aperture we have a total intensity of NUMBER and a mean intensity of NUMBER, while with the smallest aperture the total intensity and the mean intensity are respectively:NUMBER AND NUMBER. As expected the total amount of light decrease if we close the aperture, even in the post processing case. Regarding the extended depth of field achievable reducing the aperture in post processing to a single pixel, applied the home made algorithm to raw data downloaded from Stanford microscopy group. In figure 1.8 is shown the raw image of thin silky skin separating two layers of an onion, immersed in oil to improve transparency.

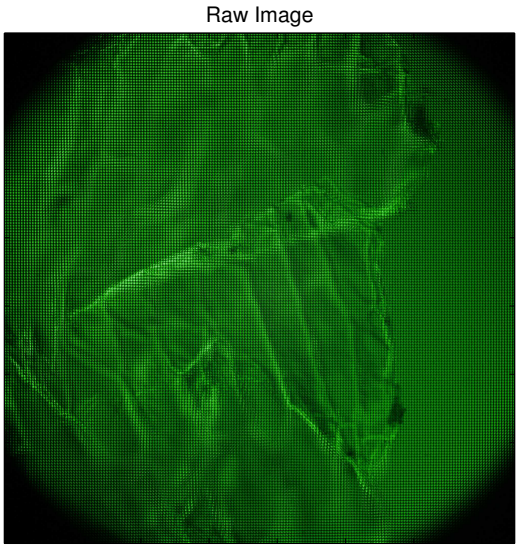

Figure 1.8: Raw plenoptic 1.0 image obatined by Marc Levoy. The microscope was a Zeiss Axiovert with a 20x/0.5NA (dry) objective. The microlens array was 24mm x 36mm, with square 125-micron x 125-micron f/20 microlenses, held in front of the Axiovert's side camera port using an optical bench mount. The camera was a Canon 5D full-frame digital SLR. The specimen was the thin silky skin separating two layers of an onion, immersed in oil to improve transparency [4].

In figure are shown the differences between the rendered image integrating over the full aperture, and the rendered image obatined using only the central pixel of each sub image. The effect is to reduce the aperture to a pinhole and to have an all-in-focus image. Images has been obtained with home made rendering algorithm written in MATLAB. parating two layers of an onion, immersed in oil to improve transparency.

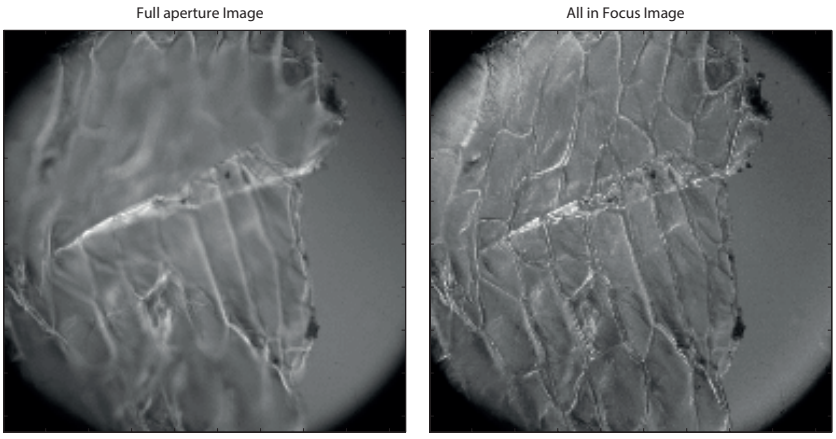

Figure 1.9: Rendered Images from the raw data in figure 1.8. On the left there is the full aperture imagea, obtained integrating along all the directional coordinates while on the right there is the all in focus image obtained taking onli the central pixel of the each sub image, that corresponds to rays with the direction parallel to the optical axis.

1.2.2 Changing point of view

It is possible to change to point of view of the rendered image integrating along he directional coordinates that correspond to a particular r point of view. Viewpoint can be chosen both in x and y direction. In this case for example, with reference to figure, if we chose to render the image as seen from the direction θ_{x1} we integrate along all the directional coordinates θ_y corresponding to θ_{x1}.

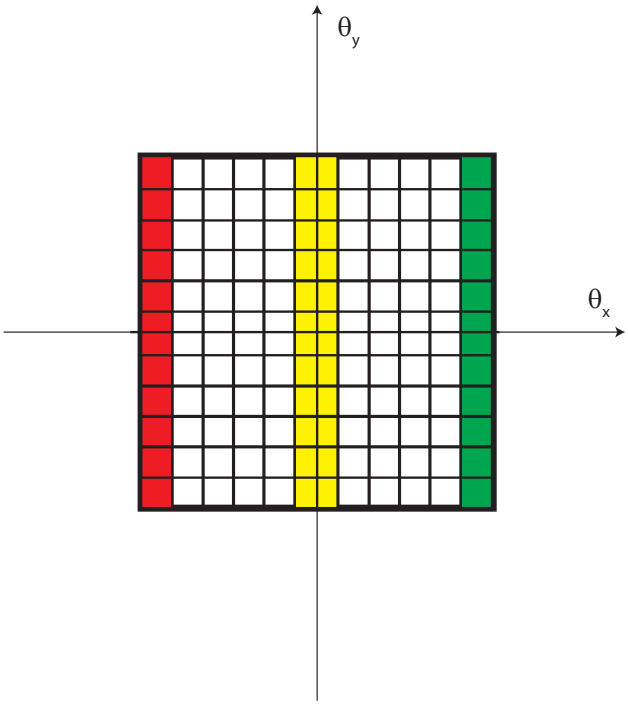

Figure 1.10: incomplete.

It is also possible to choose only one specific viewpoint (θ_x, θ_y) and rendering the image using only one single pixel per sub image. The rendering equation then becomes:

$$\begin{aligned} I(x,y) &= \frac{1}{N}\sum_{i=0}^{N} L(x,y,i,\theta_y) \\ I(x,y) &= \frac{1}{N}\sum_{j=0}^{N} L(x,y,\theta_x,j) \end{aligned} \tag{1.5}$$

1.3 Depth estimation

In this section we will explain how it is possible to extract depth information from light fields data. In the specific case of plenoptic 1.0 raw data, depth can be decoded looking at the phase space. In section **??** is explained that a point source on the focal plane of the main lens looks like a straight vertical line in

the phase space. The physical meaning of this is that for a single position, one lens let, all the directional coordinates are sampled[3]. If the point source is out of focus the situation is different. If the source is closer to the main lens respect the focal plane, it will be imaged on a plane that is behind the micro array. This situation is shown in figure 1.11. Both directional and positional coordinates are sampled by more than one lens let and each sub image will sample a set of directional coordinates correspondent to the part of the main lens from where the rays come from. In figure 1.12 it is shown what happens in the phase space. On the lens let plane the spot size will have a width of Δx proportional to the distance, therefore the directions will be sampled by the lens lets included in this interval. Each lens let receive light coming form a particular area of the main lens, its correspondent sub image only records the pixels linked with those coordinates as can be seen comparing figure 1.11 with 1.12. The resultant phase space representation is still a straight line, but with positive slope proportional to the distance of the point source 1.12. If the source is further away from the plane where the main lens is focused, the main lens image is formed before the lens lets plane. The point is still sampled by more than one lens let included in the spot size Δx. The difference with the previous case is that now in the phase space the point source is represented by a straight line with a negative slope. The physical meaning of the slope of the phase space line can be understood looking at figure 1.13. When the main lens image is formed in front of the micro lens plane the increasing directions on θ_x axis are mapped on decreasing positions on the x axis and the line on the phase space representing the point has a negative slope. If the image is formed behind the micro lens plane increasing

directions on θ_x axis are mapped on increasing positions on the x axis this inversion is absent and the line in the phase space has a positive slope [2]. This characteristic of the phase space permits to discriminate between points in the scene that are in front or behind the main lens focal plane, giving a first rough depth estimation.

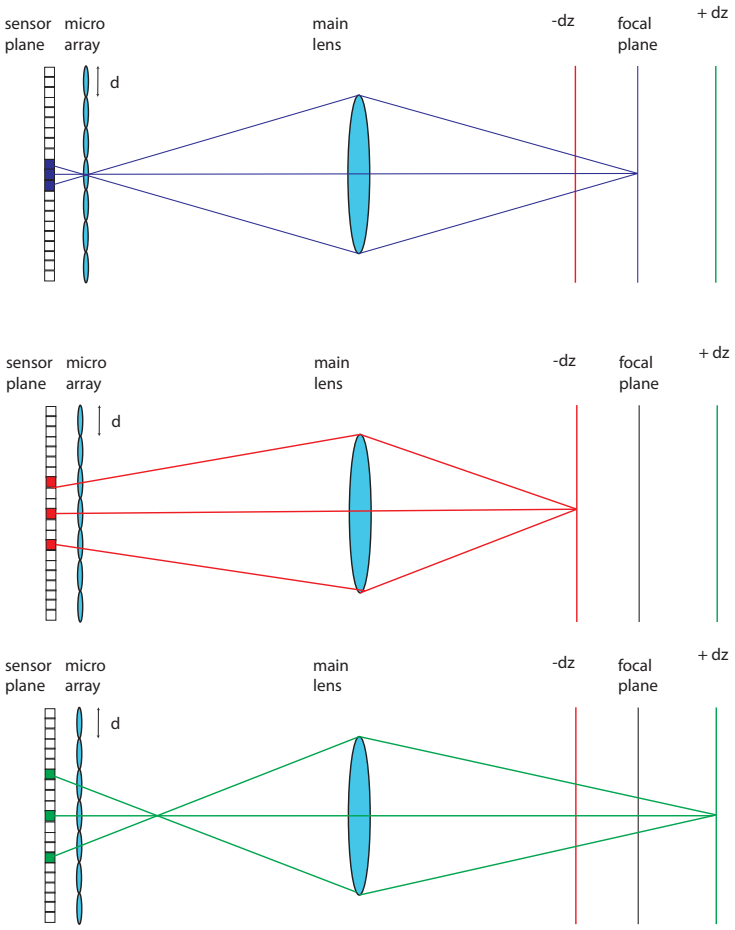

Figure 1.11: Sampling of the light field of a point source in focus, on the top, closer to the main lens, centre, and further away, bottom. When the source is out of focus, both position and directions are sampled by more than one lens let since the main lens image is not formed any more on the lens let plane.

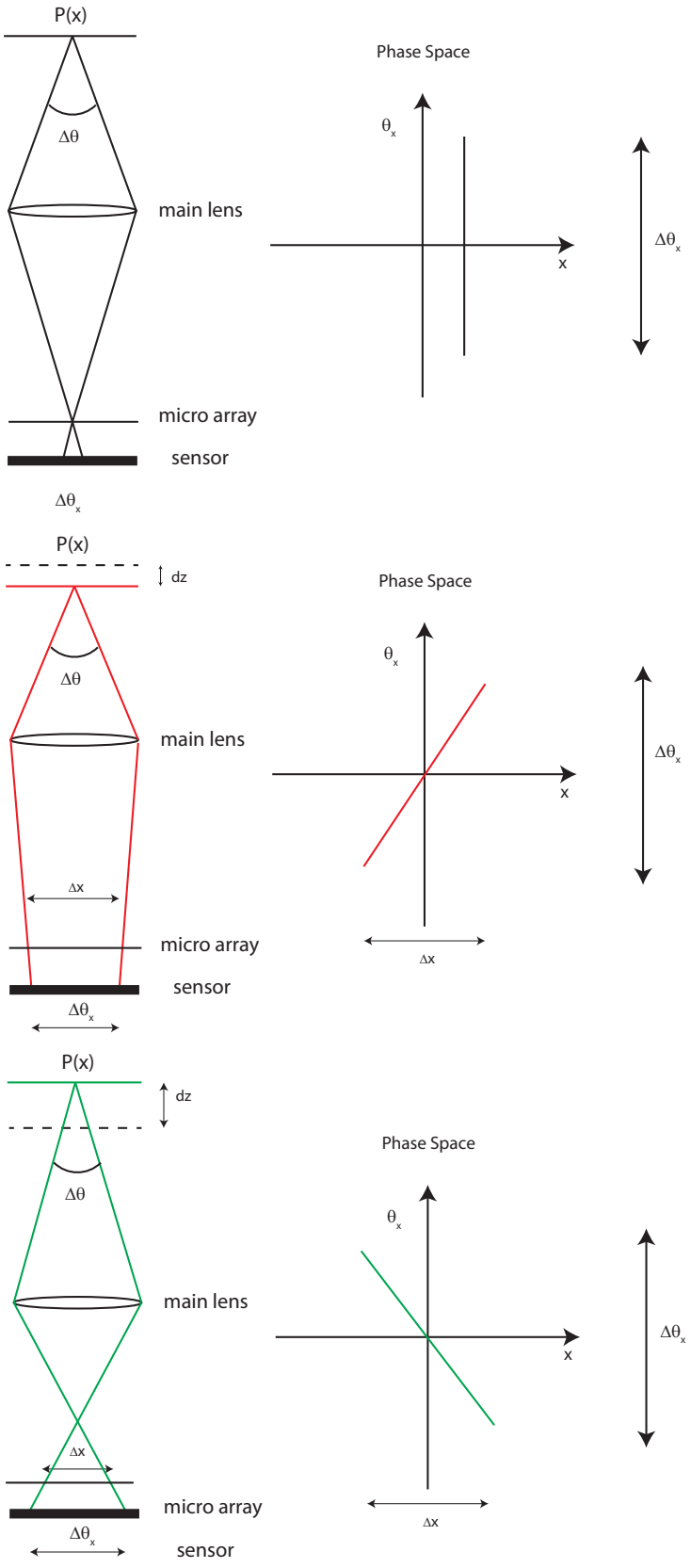

Figure 1.12: Information on the depth of a point source imaged by a plenoptic 1.0 system. As explained in section **??** If the point source is in focus, on the top, it's position is sampled by one lens let as well as the whole set of directions .

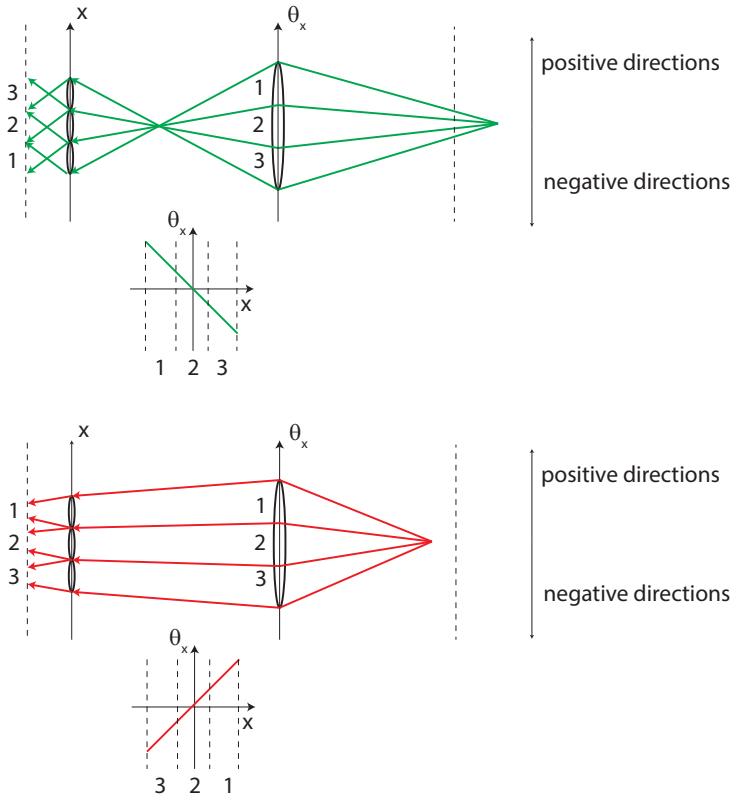

Figure 1.13: Physical meaning of the slope in the phase space. If the point source is further then the camera focal plane, the phase space line has a negative slope. If the point source is closer then the focal plane, the slope of the phase space line is positive.

A simulation of plenoptic 1.0 camera has been made to verify this fact. The system was composed by a main lens with a focal length of *120 mm*, in a *2f* configuration creating an image on the micro array plane. The Micro lens array was composed by a matrix of 101 by 101 lens lets, with a diameter of

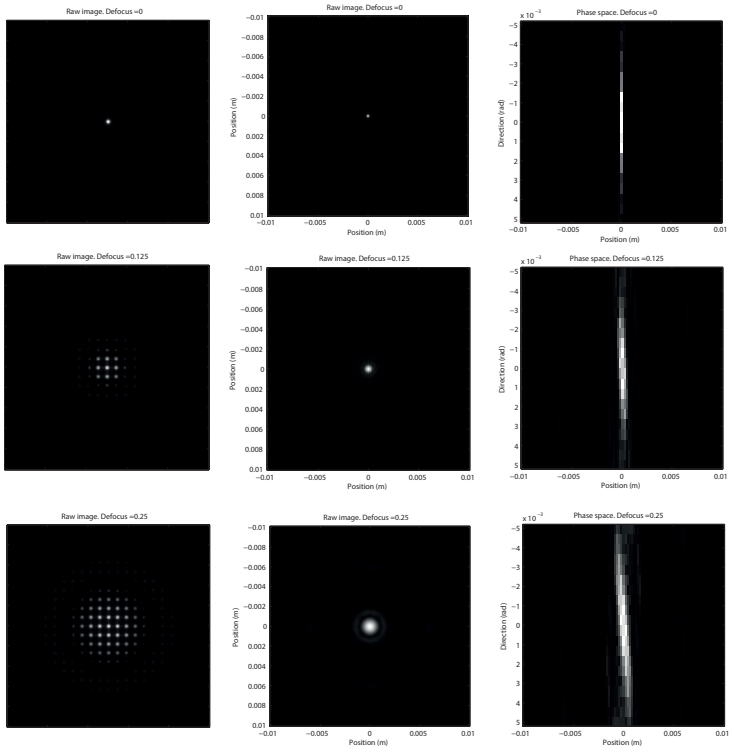

Figure 1.14: Numerical simulation of a point source imaged by a plenoptic 1.0 imaging system. The point source was placed at three different distances from the main lens. On the top we have the focused image. in the centre we have a defocus of 0.125 m far away from the main lens and on the bottom the de focus is 0.25. For these three cases we represent the raw data image, on the left, the rendered image on the center and the phase space line on the left.

1.4 Synthetic refocus

The most fascinating post processing features enabled by collecting the light field is the possibility to refocus an image after it has been captured. This features is called synthetic refocusing and is based on the fact that the recorded light field can be used to compute images as if they were taken by a synthetic camera positioned and focused differently form the actual camera. In this section we will explain a method to manipulate light field to refocus in post

processing an image. This method is based on the fact that it possible to define a synthetic camera composed by an aperture and a sensor plane, for which the defocused object plane results in focus. We will also show how this method, based on a synthetic camera model obtained with ray tracing, can be implemented in a wave optics approach, and we will discuss the limitations and the issues arising from a wave approach respect the simple and ideal ray optics approach. In figure 1.15 is shown a plenoptic 1.0 imaging system whose main lens produces an out of focus image on the micro lens plane. The directional set of coordinates Δu is mapped by along the range of spatial coordinates Δx. The light field can be re parametrized in terms of a synthetic light field generated by an aperture on the plane u' represented by the dashed lens, that focus the object on a synthetic focal plane, x'. This second light field is parametrized with the coordinates u' v' and x' y'.

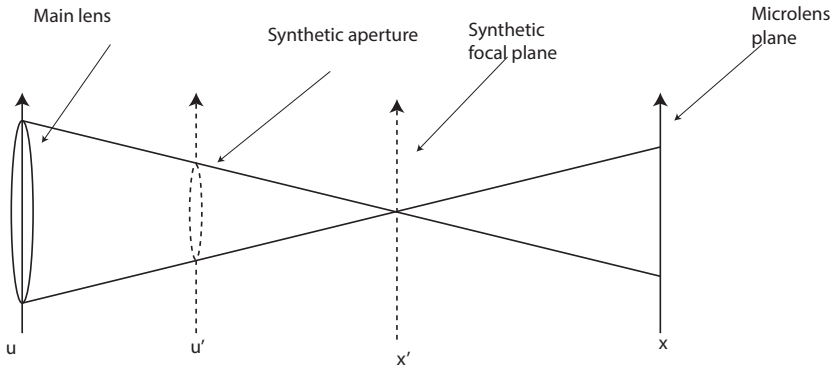

Figure 1.15: The synthetic camera refocusing method is based on the fact that is always possible to define a virtual aperture that is focused on the lens let plane.

Following the work of Ng *et al.* [10] and in analogy with what explained in section **??**, we define the intensity obtained rendering a synthetic light

field $L'(x', y', u', v')$ at the synthetic focal plane as:

$$I(x, y) = \iint L'(x', y', u', v')A(u', v')dudv \tag{1.6}$$

The goal is to express this intensity as a function of the captured light field $L(x, y, u, v)$ presente on the actual sensor plane, finding the relationship that links the set of coordinates *x,y,u,v* with *x',y',u',v'*.

1.4.1 Synthetic refocus algorithm

To find the link between the real and the synthetic light field we do the following simplifications:

- We assume that to refocus an object, only the synthetic sensor plane *x',y'* will be moved. Therefore the main lens plane *u',v'* is at the same position of the plane *u,v*, and no transformation is performed on the directional coordinates, so we can write *(u,v)=(u',v')*.

- the aperture of the main lens will not change, $A(x', y') = 1$.

In figure 1.16 is shown a two dimensional diagram explaining the re-parametrization under the hypotheses explained above. Only shows the coordinates x and u are shown for simplicity. we define F as the distance of the main lens from the lens let array plane, and F' as the distance from the synthetic focal plane. The ratio between these two distances is the refocusing parameter α, defined as:

$$\alpha = \frac{F}{F'} \tag{1.7}$$

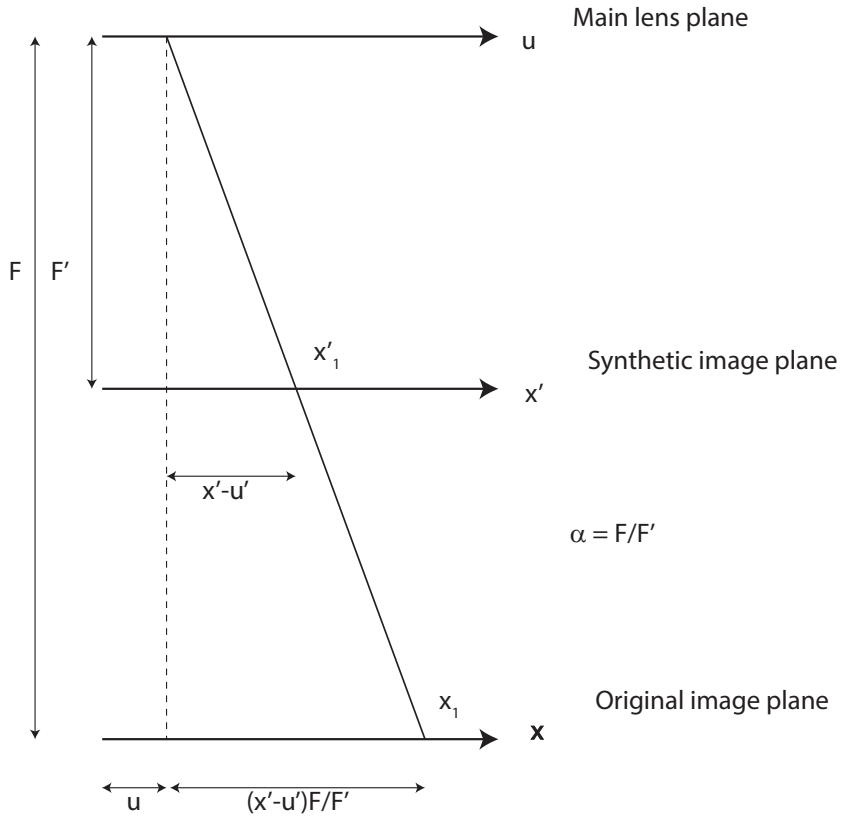

Figure 1.16: Changing the focal plane of the camera is equual to re parametrize the light field according to the new coordinates. The re parametrization is basically a shift proportional to the ratio between the refocused plane and the original camera plane α .

The refocusing factor can assume the following values:

- $\alpha = 1$ when the synthetic focal plane is at the same position of the main lens focal plane

- $\alpha > 1$ when the distance between the main lens and the synthetic image plane is smaller than the distance between the main lens and its original focal plane. This occur when we are refocusing on a plane that it further away respect the main lens focal plane.

- $\alpha < 1$ when the distance between the main lens and the synthetic image plane is bigger than the distance between the main lens and its original focal plane. This occur when we are refocusing on a plane that it closer to the main lens.

Looking at figure 1.16 we see that a ray of light that crosses the main lens plane at the coordinate u and that then intercepts the synthetic image plane at the point x_1', can be represented using with the coordinates of the original image plane x_1. Because of similar triangles, the value of the x coordinate on the image plane can be expressed as a function of the coordinates u, x'. We have:

$$x_1 = u + (x_1' - u)\frac{F}{F'} = u + (x_1' - u)\alpha \tag{1.8}$$

Therefore extending to the four dimensional case, the points belonging to the synthetic image plane can be expressed as function of the directional coordinates at the main lens plane and the spatial coordinates at the original image plane as:

$$\begin{aligned} x' &= \frac{x}{\alpha} + u\left(1 - \frac{1}{\alpha}\right) \\ y' &= \frac{y}{\alpha} + v\left(1 - \frac{1}{\alpha}\right) \end{aligned} \tag{1.9}$$

With this change of coordinates the light field at the synthetic focal plane x' can be written substituting equations 1.9 into equation 1.6.

$$I(x,y) = \iint L\left(\frac{x}{\alpha} + u\left(1 - \frac{1}{\alpha}\right), \frac{y}{\alpha} + v\left(1 - \frac{1}{\alpha}\right), u, v\right) A(x', y')dudv \tag{1.10}$$

Equation 1.10 represent the rendered image obtained integrating along the directional coordinates the light field re parametrized as if it were captured by

a camera whose focal plane is the same as the synthetic focal plane. Focusing at different depths corresponds to changing the separation between the lens and the film plane, shifting it of a quantity proportional to the refocusing factor α. From equation 1.9 we see that the four dimensional the light field at the synthetic plane is obtained from the light field recorded on the sensor by shifting and rescaling its spatial coordinates. The transformation operated on the light field is the composition of two transformations:

- a scaling of a factor α that depends by the distance of the synthetic focal plane from the main lens.
- a translation term $u(1 - 1/\alpha)$ that increases with the directional coordinates and with the magnitude of the factor alpha.

Therefore we can treat the synthetic refocus as a linear operator acting on the four dimensional light field that maps the light field recorded on a new set of coordinates. The rendering on this new set of coordinates gives the image focused at a different plane.

1.4.2 Refocusing Operator

The synthetic refocus equation 1.10 has been obtained with ray optics considerations only. However, it can be applied to light fields obtained light fields obtained with wave optics simulations. The only difference will be that particular attention should be given in the design of the imaging system in order to avoid cross talk effects induced by diffraction, as explained in section 1.1.1. The effects of this operator in the phase space is a change of the slope of the lines describing the points of the image in the phase space.

Since the total light field is conserved, the area in the phase space remains the same, hence the projection of the light field on the phase space results sheared respect the original one.

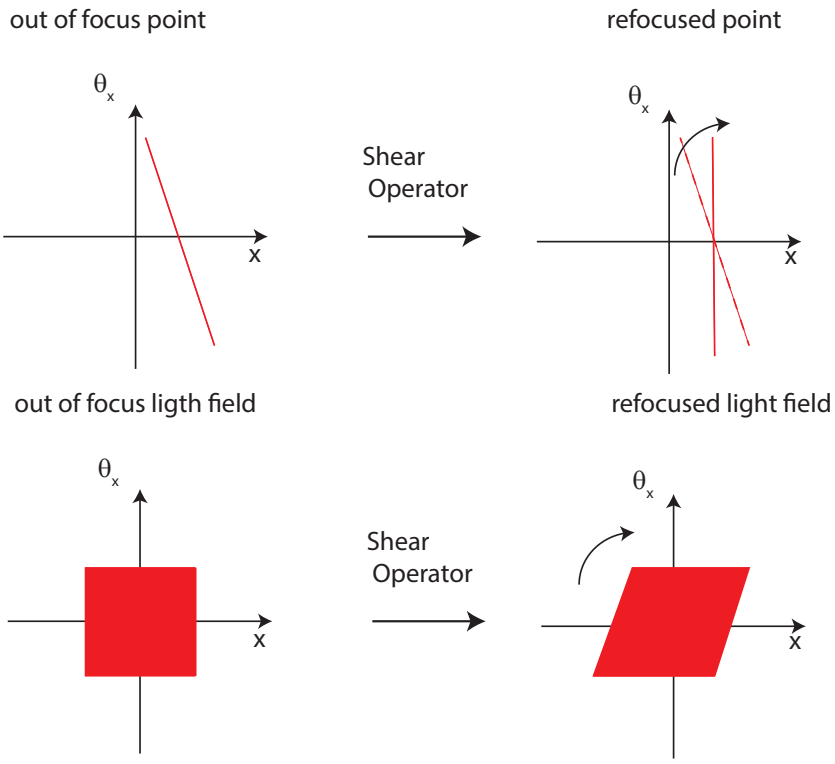

Figure 1.17: Changing the osition of the focal plane is equal to shear the light field in the phase space. The total area remains the same since the total light field is conserved.

From a computation point of view we implemented the synthetic refocus operator in MATLAB. The operator is composed by three stages. The first stage it creates a new set of spatial coordinates shifting and rescaling the the original set of coordinates as shown in equation 1.9. Then the output synthetic light field is created interpolating the input light field using as a base the new set of coordinates. The flow chart can be seen in figure 1.18

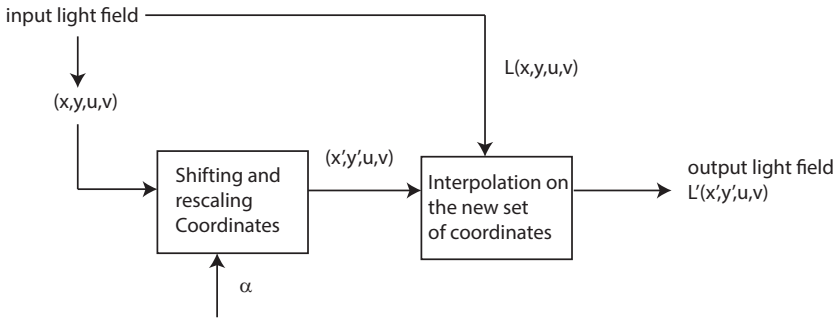

Figure 1.18: Flow chart of the operator shearing.

1.5 Results of the Simulations

To test and explore the potentials of the synthetic refocusing algorithm we generated a set of light field using the wave opticas simulation toolbox described in section **??**. The System simulated is tha one described in section **??** and shown in figure 1.19 and the optical parameters can be found in the following table.

Main lens focal length f	120mm
Lens aperture D	3.6 mm
Micro lens focal length f_μ	10 mm
Micro lens diameter d	150 μm
Micro array pitch p	150 μm
Field of view W	20 mm
f-number	33.6
sensor resolution	3030 by 3030 pixel

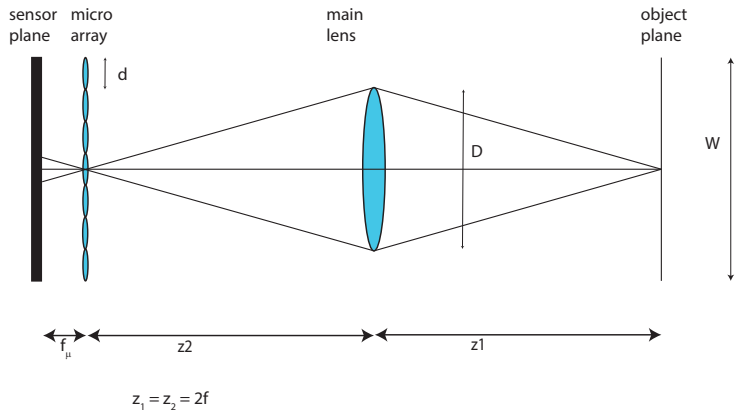

Figure 1.19: Set up simulated.

With this set up the final rendered image resolution is of 101 by 101 pixel. Each pixel of the final image corresponds to a lens let, therefore the spatial resolution the final image is equal to the diameter of the single lens let. Each sub image has 30 by 30 pixels, meaning that the full set of directional coordinates is sampled by $N_{sub} = 30$ samples. The angular resolution is therefore:

$$\delta\theta = \frac{\Delta\theta}{N_{sub}} = \frac{NA}{N_{sub}} \tag{1.11}$$

and is equal to $\delta\theta = 2.5x10^{-4}rad$.

The first object to be imaged was a volume V of dimension 20 mm x 20 mm x 100 mm containing three point sources. Each point source has been simulated by a circle of 10 μm diameter and are positioned as shown in figure 1.20

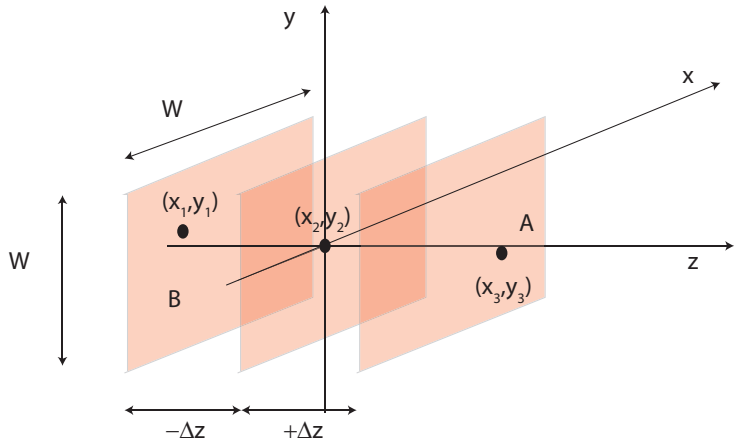

Figure 1.20: Position of the point sources imaged inside the volume V simulated.

Each plane has been imaged singularly setting the distance z_1 equal to the sum of the distance of the main lens focal plane and the defocus δz. The Coordinates of the points where:

- A: $x_1 = -3, y_1 = -3, z_1 = -50$
- B: $x_2 = 0, y_2 = 0, z_2 = 0$
- C: $x_3 = +3, y_3 = +3, z_3 = +50$

After that the light of the three planes has been propagated into the system, the final raw image has been obtained summing the three separate raw images normalized by the total amount of energy contained. This can be done since the Fresnel simulation toolbox is time independent. In figure 1.21 are shown the total raw image and the rendered image integrated without any refocusing. 1.20

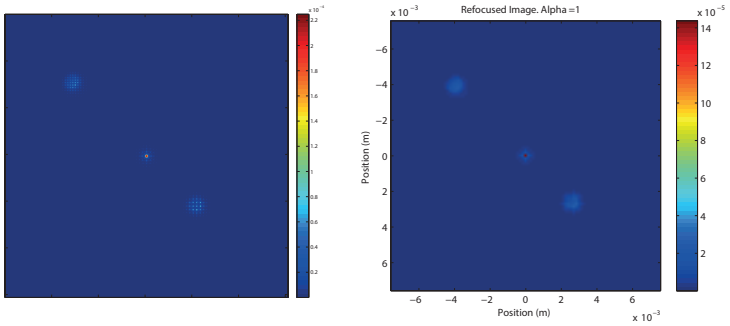

Figure 1.21: Raw image on the left and rendered image on the right. Intensity is shown in false colour in order to appreciate variations in energy distribution.

The central spot is in focus, since the point source is at a distance of $z = 2f$ on the main lens focal plane. For a defocus of 50 mm the factor α can be obtained from the lens equation. For the 2f system simulated and referring to figure 1.16 for notations, we have

$$\frac{1}{f} = \frac{1}{F'} + \frac{1}{z + \Delta z)} \tag{1.12}$$

Since $\alpha = F/F'$, and in a 2f system F=2f=z, we have:

$$\frac{1}{f} = \frac{\alpha}{2f} + \frac{1}{2f + \Delta z)} \tag{1.13}$$

Resolving for α we have:

$$\alpha = \frac{2f + s\Delta z}{2f + \Delta z} \tag{1.14}$$

In figure are shown the values of α obtained by equation1.14 for defocus varying between plus and minus 10 cm.

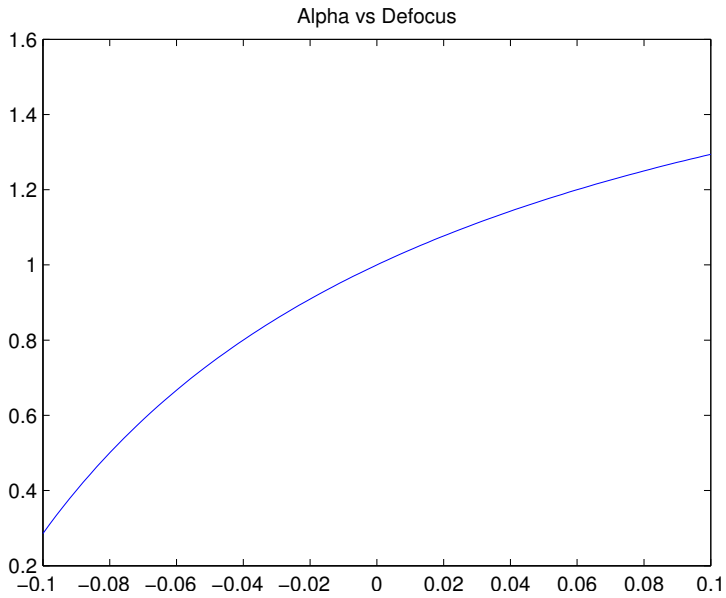

Figure 1.22: Raw image on the left and rendered image on the right. Intensity is shown in false colour in order to appreciate variations in energy distribution.

We can see from figure 1.22 that, as expected, the refocus factor is not linear with defocus and therefore the axial resolution in not linear. When the object is closer to the the main lens, small variations in the defocus give large variations in α while the opposite happen when the object is further away respect the main lens.

To conclude this section we show the refocused imaged obtained shearing the light field extracted by the raw image in figure 1.21. According to equation 1.14, the point A is refocused for a value of α equal to 0.7 and point B for $\alpha = 1.17$. Results are shown in figure 1.23

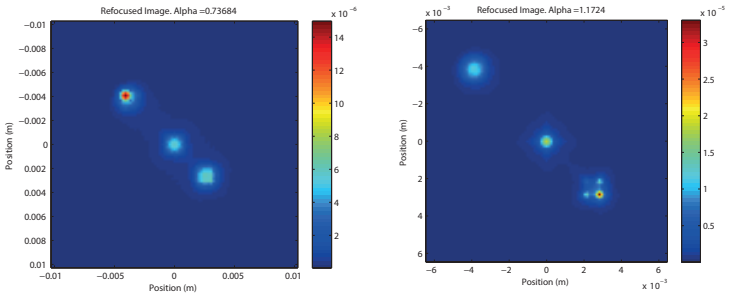

Figure 1.23: Refocused images...

1.6 Focal stack depth estimation

The synthetic refocus algorithm provides a method to estimate the depth of a point source in a volume. If we have a look at the Fourier transform of a rendered image of a point source before and after refocus, we note that when the point source is in focus, its spectrum is broader than the blurred one. This fact is true for normal images as well, when the presence of sharp details in the focused image, causes its spectrum to have a larger amount of high spatial frequencies, and therefore a bigger energy distributed on the nigh frequencies. In figure is shown the difference between the spectrum of the out of focus image(blue) and the in focus image(red) for a defocus of 5 cm.

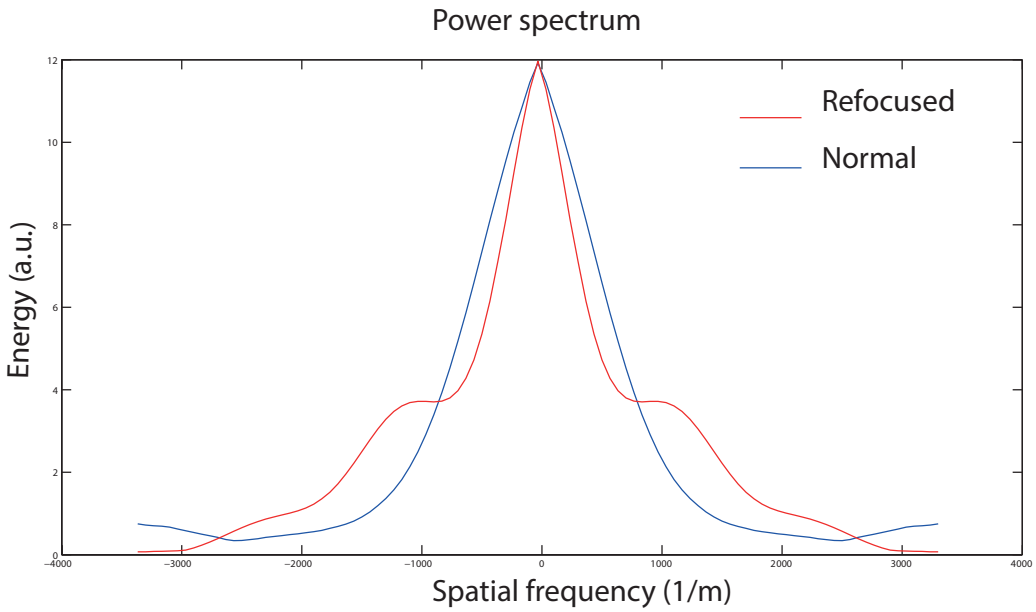

Figure 1.24: Refocused images...

The action of shearing the light field produces a redistribution of the power spectrum of the signal towards high frequency. This effect causes the sharpness of the image and therefore the refocus. This effect can be used to estimate the depth of object imaged just evaluating its level of blur. The method consist in creating a focal stack shearing the light field at different values of the coefficient alpha, that correspond to different focal planes, and rendering the images. After the focal stack is created the power spectrum of each image is calculated using the fast Fourier transform algorithm. It is then removed the low frequency terms and it calculated the total energy contained in the high frequency term. Plotting the values of energy as a function of the different alpha coefficients, we obtain a curve with presents a maximum in the proximity of the most in focus image. This maximum corresponds to the value of alpha that best estimates the actual value of alpha. In figure 1.25

are shown the energy as a function of the refus parameter alpha for a point source placed at different depths. The vertical red line indicate the position of the maximum. The values of the estimated alpha and the real one are shown in the following table:

Estimated α	Real *alpha*	Error	Defocus
0.85	0.738	0.1132	-0.05 m
0.925	0.8837	0.0413	-0.025 m
1.080	1.0943	-0.0143	+0.025 m
1.105	1.1724	0.0674	+0.05 m

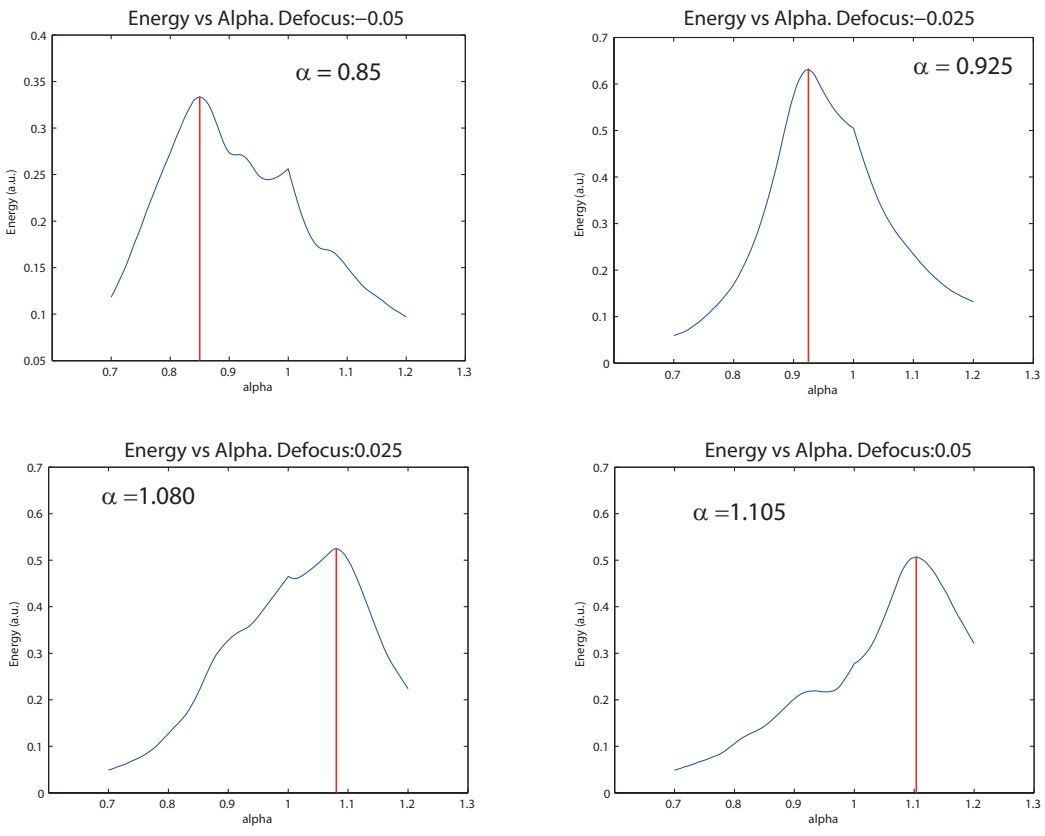

Figure 1.25: Refocused images...

In figure are shown the distribution of the estimated values of alpha in

comparison with the actual values of alpha from equation 1.14. It is clear that when the object is close to the main lens, defocus is negativ, the error in evaluating alpha is bigger, while the more accurate values are in the range of depth close to the focal plane.

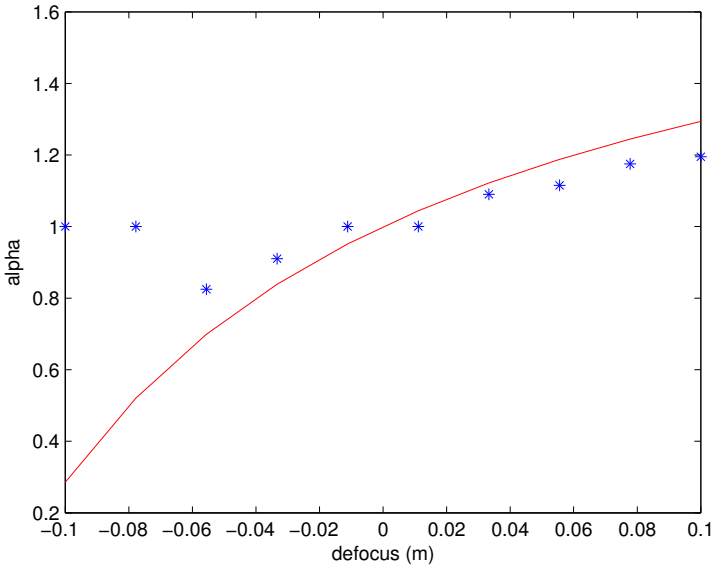

Figure 1.26: Estimated values of α represented by blea stars and the theoretical values represented with the blue line.

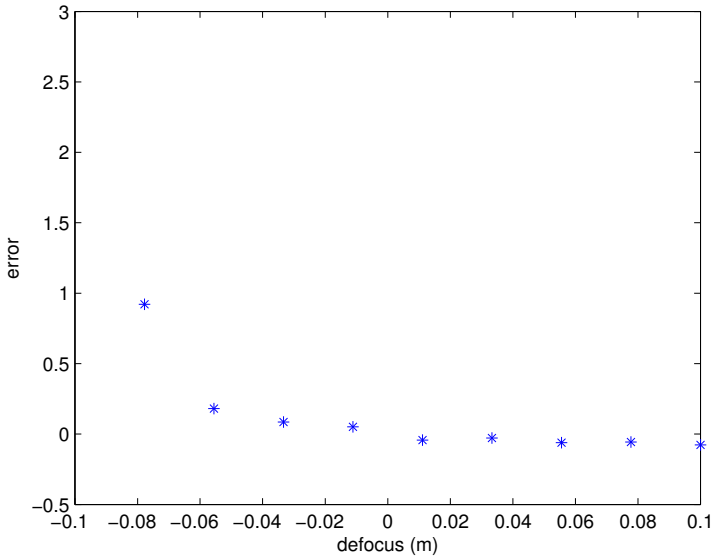

Figure 1.27: Distance between the estimated values of alpha and thje actual theoretical values.

1.7 Conclusion

Bibliography

[1] Shree K Nayar. Computational cameras: Redefining the image. *Computer*, (8):30–38, 2006.

[2] Ren Ng. *Digital light field photography*. PhD thesis, stanford university, 2006.

[3] Todor Georgiev and Andrew Lumsdaine. Focused plenoptic camera and rendering. *Journal of Electronic Imaging*, 19(2):021106–021106, 2010.

[4] Levoy Mark. Stanford light field microscope project, 2005.

[5] Changyin Zhou and Shree K Nayar. Computational cameras: Convergence of optics and processing. *Image Processing, IEEE Transactions on*, 20(12):3322–3340, 2011.

[6] Edward H Adelson and James R Bergen. *The plenoptic function and the elements of early vision*. Vision and Modeling Group, Media Laboratory, Massachusetts Institute of Technology, 1991.

[7] Edward H Adelson and John Y. A. Wang. Single lens stereo with a plenoptic camera. *IEEE Transactions on Pattern Analysis & Machine Intelligence*, (2):99–106, 1992.

[8] Marc Levoy and Pat Hanrahan. Light field rendering. In *Proceedings of the 23rd annual conference on Computer graphics and interactive techniques*, pages 31–42. ACM, 1996.

[9] Todor Georgiev and Chintan Intwala. Light field camera design for integral view photography. *Adobe System, Inc*, 2006.

[10] Ren Ng, Marc Levoy, Mathieu Brédif, Gene Duval, Mark Horowitz, and Pat Hanrahan. Light field photography with a hand-held plenoptic camera. *Computer Science Technical Report CSTR*, 2(11), 2005.

[11] Andrew Lumsdaine and Todor Georgiev. Full resolution lightfield rendering. *Indiana University and Adobe Systems, Tech. Rep*, 2008.

[12] Andrew Lumsdaine and Todor Georgiev. The focused plenoptic camera. In *Computational Photography (ICCP), 2009 IEEE International Conference on*, pages 1–8. IEEE, 2009.

[13] Victor Guillemin and Shlomo Sternberg. *Symplectic techniques in physics*. Cambridge University Press, 1990.

[14] Arnold Sommerfeld. Optics lectures on theortical physics, vol. iv. *Optics Lectures on Theortical Physics, Vol. IV by Arnold Sommerfeld New York, NY: Academic Press INC, 1954*, 1, 1954.

[15] Joseph W Goodman. *Introduction to Fourier optics*. Roberts and Company Publishers, 2005.

[16] Maciej Sypek. Light propagation in the fresnel region. new numerical approach. *Optics communications*, 116(1):43–48, 1995.

[17] Rafael C Gonzalez, Richard Eugene Woods, and Steven L Eddins. *Digital image processing using MATLAB*. Pearson Education India, 2004.

[18] Kyoji Matsushima and Tomoyoshi Shimobaba. Band-limited angular spectrum method for numerical simulation of free-space propagation in far and near fields. *Optics express*, 17(22):19662–19673, 2009.

[19] Maciej Sypek. Reply to the comment on "light propagation in the fresnel region–new numerical approach". *Optics Communications*, 282(6):1074–1077, 2009.

[20] Max Born and Emil Wolf. *Principles of optics: electromagnetic theory of propagation, interference and diffraction of light*. Cambridge university press, 1999.

[21] Joseph W Goodman and Randy L Haupt. *Statistical optics*. John Wiley & Sons, 2015.

[22] Emil Wolf. *Introduction to the Theory of Coherence and Polarization of Light*. Cambridge University Press, 2007.

[23] Frank L Pedrotti and Leno S Pedrotti. Introduction to optics 2nd edition. *Introduction to Optics 2nd Edition by Frank L. Pedrotti, SJ, Leno S. Pedrotti New Jersey: Prentice Hall, 1993*, 1, 1993.

[24] Kurt Bernardo Wolf. *Geometric optics on phase space*. Springer Science & Business Media, 2004.